Quantum Chemistry of the Oxygen Evolution Reaction on Cobalt(II,III) Oxide – Implications for Designing the Optimal Catalyst

Supporting Information

Craig P. Plaisance,*[,a] Karsten Reuter,[a] and Rutger A. van Santen*[,b,c]

[a]Chair of Theoretical Chemistry and Catalysis Research Center, Technical University of Munich, D-85747, Garching, Germany

[b]Institute for Complex Molecular Systems, Eindhoven University of Technology, 5612 AZ, Eindhoven, The Netherlands

[c]Laboratory of Inorganic Materials Chemistry, Schuit Institute of Catalysis, Eindhoven University of Technology, 5612 AZ, Eindhoven, The Netherlands

*corresponding authors

Details of quantum chemical calculations *(reproduced from ref. 1)*

All quantum chemical calculations were performed with spin-polarized Kohn-Sham density functional theory (DFT) in the Vienna ab-Initio Simulation Package (VASP).[2,3] The Kohn-Sham orbitals were constructed in a plane-wave basis with an energy cutoff of 400 eV. The projector augmented wave (PAW) method[4,5] was used to describe these orbitals in the core regions. The exchange correlation energy was calculated in the generalized gradient approximation using the revised Perdew-Burke-Ernzerhof functional.[6] An additional on-site self-interaction correction was applied to the Co *3d* orbitals using the rotationally invariant implementation by Liechtenstein *et al*.[7] The rotationally averaged effective Coulomb integral (U–J) was calculated using the method detailed in the next section. Calculations on the (001) and (311) surfaces were performed only at the Γ-point while calculations on the (110) surface used a 2×1×1 Γ-centered k-point mesh. Calculations on the bulk structure used a 2×2×2 Γ-centered k-point mesh. Population of the Kohn-Sham orbitals was determined using an error-function distribution with a width of 0.02 eV on the (001) and (110) surfaces. A width of 0.2 eV was used on the (311) surface due to the presence of a hole in the valence band on the bottom of the slab.

The Kohn-Sham orbitals were determined using an iterative procedure based on the blocked Davidson scheme.[8] The charge density was determined at each step using the Pulay mixing scheme[9] with a mixing fraction of 0.1 for the total charge density and 0.4 for the magnetization density. A tolerance of 10^{-4} eV was used for determining the convergence of the Kohn-Sham orbitals and charge density. Geometries of minimum energy structures were obtained using a conjugate gradient algorithm. Convergence was achieved when all atomic forces were below 0.05 eV/Å.

One important consideration for the DFT calculations is to ensure that the electronic structure converges to the appropriate ground state. This is due to the fact that all of the surfaces have Co cations in multiple oxidation states (+II – +V) so that different meta-stable electronic states exist with different arrangements of the oxidation states. Since all of the oxidation states except Co(III) have magnetic moments, multiple magnetic states exist as well. We have taken care to make sure that we obtain the true electronic and magnetic ground state for all structures.

In order to force the calculation to converge to a particular ground state, the magnetic moments of the Co cations used to construct the initial charge density are specified. Co(II) cations in the tetrahedral sites are in the high-spin state and are assigned an initial magnetic moment of 3 μ_B. Co(III) and Co(IV) cations in octahedral sites are in the low-spin state and are assigned initial magnetic moments of 0 and 1 μ_B, respectively. In many cases, it was necessary to fine-tune the initial magnetic moments of the Co(IV) cations to obtain the correct electronic state – too low of a magnetic moment would converge to a Co(III) with the hole occupying the O 2p band and too high of a magnetic moment would converge to an intermediate-spin Co(IV). The method for determining the Co oxidation state is given in a later section.

In surfaces with Co(V)=O species, it was also necessary to specify an initial magnetic moment for the oxygen atom. These species can exist either in a triplet state where the Co and O have parallel spins of 1 μ_B or in a singlet state where the Co and O have opposite spins of 1 μ_B. For the singlet state, it was usually necessary to fine-tune the initial (spin-down) magnetic moment on the oxygen since too low of a magnetic moment would lead to the triplet state and too high of a magnetic moment would cause the spin to flip on the Co from up to down, also leading to a triplet state. In surfaces with superoxo species, it was also necessary to set the initial magnetic moments on both oxygen atoms to 1 μ_B.

The transition states for the O–O bond formation step during water addition were determined using a special procedure detailed in a following section due to the electronic transition that occurs at the transition state. The transition state for the proton coupled electron transfer (PCET) step on the (110)-A surface was found using the dimer method.[10]

The Co_3O_4 bulk unit cell used to construct the surfaces was cubic and had the composition $Co(II)_8Co(III)_{16}O_{32}$. The optimized lattice parameter was found to be 8.16 Å, which is only slightly larger than the experimental value of 8.08 Å.[11]

Determining free energies of intermediates *(reproduced from ref. 1)*

To determine the free energies of the different intermediates in the catalytic cycle, we use an approach similar to that of Nørskov and Rossmeisl in which the free energy of a proton and electron is determined by use of a reference reaction.[12,13] The most commonly used reference reaction is the hydrogen evolution reaction whereby the proton and electron are in equilibrium with H_2 gas at 1 bar. A more convenient choice for this study is to use the OER itself as the reference reaction so that the proton and electron are in equilibrium with O_2 at 1 bar and liquid water

(1)

$$2\,H_2O \rightleftharpoons O_2 + 4\,(H^+ + e^-)$$

At the potential where this reaction is in equilibrium (overpotential of zero), the free energy of the proton and electron is equal to

(2)

$$G°(e^- + H^+) = \frac{1}{2}G°(H_2O) - \frac{1}{4}G°(O_2)$$

Due to the poor description of the O_2 molecule in DFT,[13,14] we use H_2 gas as the reference along with the experimental free energy of the OER, which is 4.92 eV under standard conditions so that

(3)

$$G°(e^- + H^+) = \frac{1}{2}G°(H_2) + 1.23\ eV$$

When the overpotential is non-zero, the free energy of the proton and electron is simply increased by the overpotential (η) multiplied by the elementary charge

(4)

$$G(e^- + H^+) = G°(e^- + H^+) + e\eta$$

Since we only consider neutral systems in this study, it is not required to know the free energies of the proton and electron separately.

The other species for which a reference free energy is needed is liquid water. To get this value, we use the energy of water in the hexagonal ice structure at 0 K calculated by the same computational methods used throughout this study. The unit cell parameters used for this calculation (after relaxation) were a = 7.82 Å and c = 8.63 Å and the cell contained 8 water molecules. The results of this calculation give a cohesive energy of 0.50 eV per H_2O. Using the cohesive energy of ice at 0 K rather than the experimental free energy of vaporization of water at standard conditions is reasonable because we do not include thermal effects in any of the other calculations in this work.

Location of transition states for water addition *(reproduced from ref. 1)*

The charge transfers that occur during the water addition reaction present a particular challenge to the typically used methods of locating transition states such as the nudged elastic band[15] and dimer[10] methods. This is because the transition state (TS) is located at the crossing of two potential energy surfaces so that it is not a stationary point on either surface. In order to locate this crossing, we calculate the energy of the system at several points along the minimum energy pathway in the vicinity of the TS on both potential energy surfaces. We then chose the O−O bond distance as a reaction coordinate and find the value of this reaction coordinate where the two potential energy surfaces have the same energy. This point corresponds to the TS. This procedure is carried out in the following steps which are illustrated in Scheme S1:

1. Set up an 8-image nudged elastic band (NEB)[16] calculation with the initial images interpolated between the reactant and product using the linear synchronous transit method.[17]
2. Locate in the initial images the points where the electron transfers are likely to occur. For water addition to a bridging oxo at a dual-Co site, two electron transfers occur. The first electron transfer is estimated to occur when the proton being transferred from the attacking water to the η-OH on the surface is halfway between the two oxygen atoms. The second electron transfer is estimated to occur when the O−O bond length of the hydroperoxo being formed is 2.00 Å. For water addition to a terminal oxo at a single-Co site, only one electron transfer occurs. This electron transfer is estimated to occur when the O−O bond length is 2.00 Å.
3. Based on the estimated points of electron transfer along the NEB chain, assign a charge state to each of the images. Set the initial charge density of each image to correspond to the assigned charge state using the method described in "Details of quantum chemical calculations".
4. Perform the NEB calculation using the initial charge densities for the images obtained in the previous step. Convergence is achieved when all atomic forces in all images are below 0.3 eV/Å. A spring force constant of 5 eV/Å^2 was used.
5. From the results of the NEB, find the two images I_a and I_b on either side of the expected TS (see Scheme S1). The TS is estimated as the point where the O−O bond is 2.00 Å. If one of these two images is too close to the transition state (the O−O bond is between 1.90 Å and 2.10 Å) chose the next closest image.
6. Perform a geometry optimization on I_a with the distance to I_b fixed. Do the same for I_b with the distance to I_a fixed. The geometries are converged when all atomic forces are below 0.05 eV/Å. These new images are R_a and P_b, respectively. This step is necessary because the NEB calculation was converged to only 0.3 eV/Å.
7. Linearly interpolate between R_a and P_b three points with O−O bond lengths of 1.90 Å, 2.00 Å, and 2.10 Å. These points are I_1, I_2, and I_3, respectively. Using the charge density of R_a as the initial guess, optimize the geometries of all three structures keeping the distance to P_b fixed. The resulting structures are R_1, R_2, and R_3. Do the same using the charge density of P_b as the initial guess and keeping the distance to R_a fixed. These optimized structures are P_1, P_2, and P_3. A convergence criteria of 0.05 eV/Å is used in all optimizations. If any of the optimizations diverge, try using the other endpoint (R_a or P_b) as the fixed point for that particular structure.
8. Plot the energy versus the O−O bond distance in the optimized structures for R_1, R_2, and R_3 as well as for P_1, P_2, and P_3. Fit a parabola to each of the two sets of points. The TS is the point where the parabolas intersect.

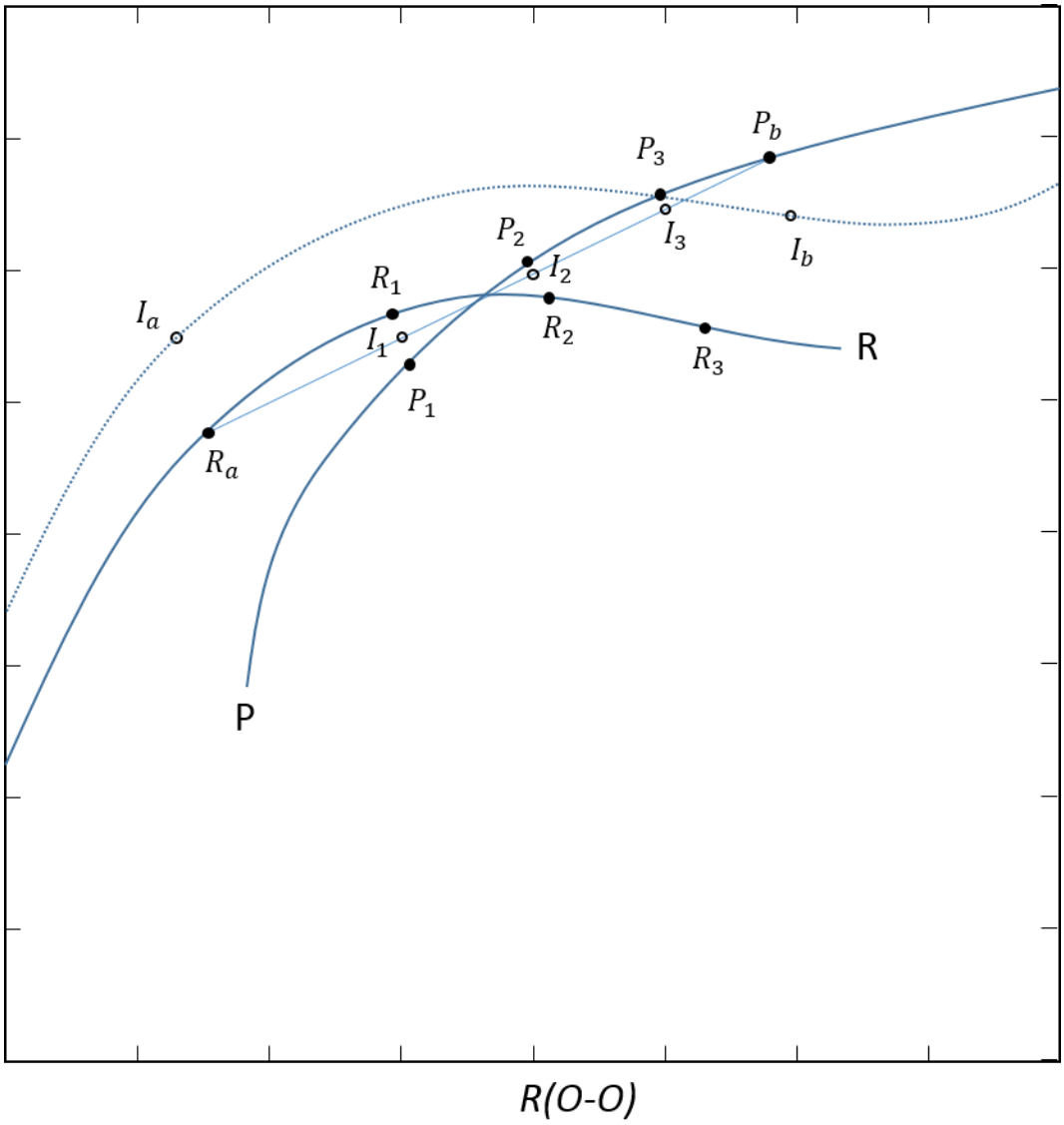

Scheme S1. Illustration of the procedure for locating the transition state of the water addition reaction on a 2-D potential energy surface. The horizontal coordinate is the O−O bond distance and the vertical coordinate is an arbitrary orthogonal reaction coordinate. The dotted line is the minimum energy path found by the (roughly converged) nudged elastic band method. The dark solid lines are the minimum energy paths for the electronic state of the reactant (R) and product (P). The points along these lines are explained in the text.

We should note that even though the O−O bond distance is the same in the structures on both potential energy surfaces at the TS, the other coordinates may not be the same. A more accurate treatment would perform a vibrational mode analysis on the two structures in order to construct a quadratic approximation of the two potential energy surfaces in the vicinity of the transition state. One could then determine the minimum energy point where the two surfaces cross in the complete coordinate space. We find, however, that the structures are very similar on the two potential energy surfaces at the transition state determined by the approximate method so that the more accurate treatment is likely not necessary. This implies that

the minimum energy pathways on the two surfaces, shown schematically in Scheme S1, largely coincide in the region of the TS.

Another point that should be made is that the crossing of the two potential energy surfaces at the TS is artificial – in reality, they would mix in the vicinity of the crossing and a gap would open between the two new potential energy surfaces. In that case, the TS would correspond to a saddle point on the new low energy PES. With the GGA+U method, however, this mixing of the two PES is suppressed because the mixed PES would involve a mixing between the Co(III) and Co(IV) states so that one of the *d* orbitals would have a fractional occupancy. The U correction penalizes such a fractional occupancy enough that the mixed-valence state is higher in energy than both of the single-valence states at the TS. This is related to the convex shape of the curve relating energy to the number of electrons in a system at fractional number of electrons in the Hartree-Fock method[18] – the self-interaction correction has a similar effect to including Fock exchange. This would seem to imply that our barriers may be overestimated. Ultimately, this is a very difficult TS to model due to the near-degeneracy of the two electronic states in its vicinity and the resulting strong static correlation.

Modeling Approximate Solvent Interactions

Solvation effect on the reaction barriers for water addition have been accounted from in an approximate way by allowing one or two additional water molecules to interact with the transition state structures. One additional water was used for sites on both the (311) and (110)-A surfaces and two additional waters were used for the site on the (110)-B surface. Two water molecules were used on the latter surface rather than one because the hydroxyl generated from the attacking water only interacts with one water ligand on this surface compared to two water or hydroxo ligands on the other two surfaces. This way, the oxygen of the hydroxyl forms three hydrogen bonds on all surfaces.

When calculating the interaction energy between the additional water and the transition state, only the water molecules were allowed to relax during geometry optimization, while the other atoms were frozen in the positions determined in the absence of the additional water. For transition states that involve a crossing between two potential energy surfaces (all except transition states except for the PCET transition state on the (110)-A site), the interaction energy with the additional water molecules was determined for both electronic configurations. The interaction energies, which are listed in Table S1, are then added to the energies used to define the potential energy profiles in step 8 of the method discussed in the previous section used to determine the crossing points. Structures of the transition states with the added water are shown in Figure S1.

Table S1. Interaction energies between transition state structures for water addition and additional water molecules on the three surfaces

	(311)	(110)-A (PCET)[d]	(110)-A (O-O)[e]	(110)-B
II[a]	-0.08		-0.13	-0.24
III[b]	-0.05		-0.05	-0.19
$\Delta E(TS)$[c]	-0.05	-0.18	-0.11	-0.18

[a] initial electronic configuration, [b] final electronic configuration, [c] change in activation barrier, [d] transition state for PCET, [e] transition state for O-O bond formation

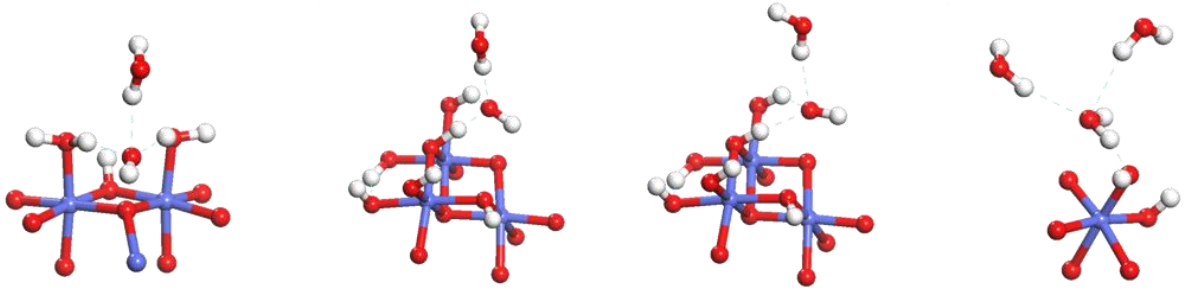

Figure S1. Structures of transition states for water addition with additional water molecules

Electronic structure analysis *(reproduced from ref. 1)*

Analysis of electronic structure was done using the Quasiatomic Orbital (QO) method developed by Qian *et al.*[19] and implemented by us in VASP. The method allows for the transformation of the Bloch orbitals from a plane wave basis to a minimal atomic orbital basis (the quasiatomic orbitals or QOs) that contains the complete subspace of occupied Bloch orbitals. The set of *N*+*M* quasiatomic orbitals $\{\phi_{\mu k}\}$ is constructed as a linear combination of *N* occupied Bloch orbitals $\{\psi_{nk}^{occ}\}$ and a set of *M* auxiliary Bloch orbitals $\{\psi_{mk}^{aux}\}$.

(5)

$$|\phi_{\mu k}\rangle = \sum_n \Omega_{n\mu}^k |\psi_{nk}^{occ}\rangle + \sum_m \Omega_{m\mu}^k |\psi_{mk}^{aux}\rangle$$

(6)

$$\Omega_{n\mu}^k = \langle \psi_{nk}^{occ} | a_{\mu k} \rangle$$

(7)

$$\Omega_{m\mu}^k = \langle \psi_{mk}^{aux} | a_{\mu k} \rangle$$

The expansion coefficients $\Omega_{n\mu}^k$ and $\Omega_{m\mu}^k$ are the projections of the Bloch orbitals on a set of *N*+*M* atomic orbitals $\{a_{\mu k}\}$. The auxiliary Bloch orbitals are orthogonal to the occupied Bloch orbitals and are the set that maximizes the overlap between the QOs and the corresponding atomic orbitals defined by the following quantity

(8)

$$\sum_\mu |\langle \phi_{\mu k} | a_{\mu k} \rangle|^2$$

The resulting set of QOs has the property of having maximum similarity to the atomic orbitals (defined by the above overlap quantity) while still containing the entire space of occupied Bloch orbitals. Because of this constraint, the QOs provide a description of the ground state properties of the system that is exactly equivalent to the description in the original plane wave basis. In practice, it is found that the QOs exhibit only small deviations from the atomic orbitals used for the fitting so that they provide an excellent basis for determining atomistic quantities such as partial charges, magnetic moments, and bond overlaps.

The QOs for the structures in this work are determined using an atomic orbital basis consisting of the *1s* orbital on H, the *2s* and *2p* orbitals on O, and the *4s* and *3d* orbitals on Co. It is found that inclusion of the Co *4p* orbitals does not lead to a significantly closer fit between the QOs and the original atomic orbitals. This indicates that the Co *4p* orbitals are not necessary to describe the ground state properties of this system – they are closer to Rydberg orbitals than valence orbitals.

Once the set of QOs is determined, the Bloch orbitals can be transformed to this basis from the original plane wave. Before doing this, it is useful to first form a set of orthonormal QOs $\{\tilde{\phi}_{\mu k}\}$ using the symmetric orthogonalization method of Löwdin[20]

(9)

$$\left|\tilde{\phi}_{\mu k}\right\rangle = \sum_{\nu} T^{k}_{\mu\nu} \left|\phi_{\nu k}\right\rangle$$

(10)

$$T^{k} = \left(S^{k}\right)^{-\frac{1}{2}}$$

where S^k is the overlap matrix between the QOs defined as

(11)

$$S^{k}_{\mu\nu} = \left\langle \phi_{\mu k} \middle| \phi_{\nu k} \right\rangle = \sum_{n} {\Omega^{k}_{n\mu}}^{*} \Omega^{k}_{n\nu} + \sum_{m} {\Omega^{k}_{m\mu}}^{*} \Omega^{k}_{m\nu}$$

The orthonormalized QOs can be written in terms of the Bloch orbitals by transforming the matrix Ω^k by T^k

(12)

$$\left|\tilde{\phi}_{\mu k}\right\rangle = \sum_{n} \widetilde{\Omega}^{k}_{n\mu} |\psi^{occ}_{nk}\rangle + \sum_{m} \widetilde{\Omega}^{k}_{m\mu} |\psi^{aux}_{mk}\rangle$$

(13)

$$\widetilde{\Omega}^{k}_{n\mu} = \sum_{\nu} T^{k}_{\mu\nu} \Omega^{k}_{n\nu}$$

(14)

$$\widetilde{\Omega}^{k}_{m\mu} = \sum_{\nu} T^{k}_{\mu\nu} \Omega^{k}_{m\nu}$$

Unlike Ω^k, $\widetilde{\Omega}^k$ is a unitary matrix so that the occupied Bloch orbitals can easily be written in the basis of orthonormalized QOs

(15)

$$|\psi^{occ}_{nk}\rangle = \sum_{\mu} {\widetilde{\Omega}^{k}_{n\mu}}^{*} \left|\tilde{\phi}_{\mu k}\right\rangle$$

Finally, we can then calculate the density matrix in the orthonormalized QO basis according to

(16)

$$P^{k}_{\mu\nu} = \sum_{n} f_{n} {\widetilde{\Omega}^{k}_{n\mu}}^{*} \widetilde{\Omega}^{k}_{n\nu}$$

where f_n is the occupancy of Bloch orbital ψ_{nk} in the case of fractional occupancies.

Up to this point, the QOs still have the periodicity of the unit cell, leading to the index k. It is more useful is we transform to a completely local basis using the Bloch transformation

(17)

$$\left|\tilde{\phi}_{\mu R}\right\rangle = \sum_{k} e^{ikR}\left|\tilde{\phi}_{\mu k}\right\rangle$$

This results in a density matrix

(18)

$$P_{\mu\nu}^{RR'} = \sum_{k} e^{ik(R-R')} P_{\mu\nu}^{k}$$

Due to the periodicity of the system, this density matrix is also periodic and depends only on the difference $R - R'$.

Determining oxidation states of Co *(reproduced from ref. 1)*

Determining the oxidation state of an atom which is part of a larger system from a quantum chemical calculation is not trivial. This is due to the sharing of electrons between atoms which leads to fractional occupancies of atomic orbitals. One possibility is to correlate the oxidation state with the partial charge using calculations on reference systems having a known oxidation state. However, this correlation does not always hold. For example, in bulk Co_3O_4, the Co cations in the tetrahedral sites are known to have an oxidation state of +II while those in the octahedral sites have an oxidation state of +III. In our calculations, though, the partial positive charge is higher on the Co(II) (1.26) than the Co(III) (1.16). This is due to the greater number of oxygen anions coordinating the Co(III) in the octahedral site compared to the Co(II) in the tetrahedral site. These oxygen anions donate electron density onto the Co, leading to a decrease in the positive partial charge.

We have developed a more robust method of determining the oxidation state based instead on the populations of the individual atomic *d* orbitals on the Co cations. The oxidation state is determined from the number of *d* orbitals that are close to being fully occupied. Co(II) has seven such orbitals, Co(III) has six, Co(IV) has five, and Co(V) has four. The number of fully occupied *d* orbitals is determined by diagonalizing the density matrix of each spin component projected on the basis of five *d* quasi-atomic orbitals on the Co. The *d* orbitals with fractional occupancy are not included because the fractional occupancy originates from donation by the oxygen ligands in the coordination shell. Therefore, these electrons are formally assigned to the ligands. There is one 5×5 atomic density matrix for each spin component and the number of occupied *d* orbitals is determined by the number of eigenvalues greater than a certain cutoff. We find that 0.90 is an acceptable cutoff which works in nearly all cases. In most cases, the occupancy of the "occupied" orbitals is greater than 0.95. The formal magnetic moment can also be determined in this way – it is simply equal to the difference in the number of spin up and spin down eigenvalues greater than the cutoff.

Method for extracting hole densities from quantum chemical calculations

The orbitals used to generate the hole densities in several of the figures in the main text were constructed from linear combinations of unoccupied Bloch orbitals in the QO representation. The particular linear combination was chosen to maximize the hole density on a given atom or set of atoms. To do this, the QOs centered on the atom or set of atoms on which the hole is to be localized are projected onto the unoccupied Bloch orbitals by multiplication with the hole density matrix Q

(19)

$$\left|\tilde{\phi}_{\mu 0}\right\rangle_Q = \sum_{R\nu} Q_{\mu\nu}^{0R} \left|\tilde{\phi}_{\nu R}\right\rangle$$

with Q defined from the density matrix P in eq. (18) by

(20)

$$Q_{\mu\nu}^{RR'} = \delta_{\mu\nu}\delta_{RR'} - P_{\mu\nu}^{RR'}$$

The Hamiltonian and overlap matrices are then constructed in the basis of these projected QOs

(21)

$$H_{\mu\nu} = \left\langle \tilde{\phi}_{\mu 0} \middle| \widehat{H}_{KS} \middle| \tilde{\phi}_{\nu 0} \right\rangle_Q$$

(22)

$$S_{\mu\nu} = \left\langle \tilde{\phi}_{\mu 0} \middle| \tilde{\phi}_{\nu 0} \right\rangle_Q$$

where $\widehat{H}_{KS}$ is the Kohn-Sham Hamiltonian operator taken from the DFT calculation. We then solve the generalized eigenvalue problem in the basis of projected QOs

(23)

$$\sum_{\nu} H_{\mu\nu} c_\nu^i = \varepsilon_i \sum_{\nu} S_{\mu\nu} c_\nu^i$$

where c_ν^i are the elements of the ith eigenvector with eigenvalue ε_i. The localized orbital(s) containing the hole(s) are taken from the eigenvector(s) j that most closely match the expected shapes

(24)

$$|\psi_{hole}\rangle = \sum_{\nu} c_\nu^j \left|\tilde{\phi}_{\nu j}\right\rangle_Q$$

In addition to the orbital(s) containing the hole(s), there are two eigenvectors corresponding to the empty *3d* e_g orbitals on each Co cation included in the localization basis. In all cases, it was trivial to distinguish these and exclude them.

The localization basis used in each of the figures in the main text are given below:

Figure 3 - 5: oxo, neighboring octahedrally coordinated Co cations, and oxygen of attacking water

Figure 6: three structures in top row of diagram for each site – same as in Figures 3 - 5

Figure 9: hole in O-H bond formation product – oxo, added hydrogen, and neighboring octahedrally coordinated Co cations

A similar method is used to determine the lone pair orbitals used to plot densities in Figure 8 of the main text except the density matrix P is used to form the projected QOs rather than the hole density matrix Q. The four QOs on the oxo are used as the localization basis. The generalized eigenvalue problem in eq. (23) is solved and the eigenvector corresponding to the orbital containing the hole is excluded while the remaining three eigenvectors are used to construct the delocalized lone pair density.

Method for quantifying the number of electrons donated in hydrogen bonds

In the main text, the number of electrons donated in hydrogen bonds to the hydroxyl intermediate formed during water addition was specified. To determine this quantity, we take the elements of the density matrix given in eq. (18) between the QOs on the donor oxygen atom A and the *1s* QO on the acceptor hydrogen. The donor orbital on the oxygen is then defined by this vector

(25)

$$|D^0\rangle = \frac{1}{\sqrt{N^0}} \sum_{\mu \in A} P_{\mu s}^{00} |\tilde{\phi}_{\mu 0}\rangle$$

$$N^0 = \sum_{\mu \in A} \left(P_{\mu s}^{00}\right)^2$$

where the sum is over all QOs on the donor oxygen. Since the donor orbital is also partially delocalized onto the other atoms neighboring the donor oxygen, we must project $|d^0\rangle$ onto the occupied Bloch states by multiplication with the density matrix and normalization

(26)

$$|D\rangle = \frac{1}{\sqrt{N}} P|D^0\rangle = \frac{1}{\sqrt{N^0 N}} \sum_{R\nu} \left(\sum_{\mu \in A} P_{\nu\mu}^{R0} P_{\mu s}^{00} \right) |\tilde{\phi}_{\nu 0}\rangle$$

$$N = \langle D^0 | P^2 | D^0 \rangle = \langle D^0 | P | D^0 \rangle$$

The number of electrons donated in the hydrogen bond is equal to the population of this donor orbital on the hydrogen *1s* QO, which is equal to the following after making use of the definition of N^0 in eq. (25)

(27)

$$n = \langle D | \tilde{\phi}_{s0} \rangle = \frac{1}{N^0 N} \left(\sum_{\mu \in A} \left(P_{\mu s}^{00}\right)^2 \right)^2 = \frac{N^0}{N}$$

Intermediate states of the (110)-A surface

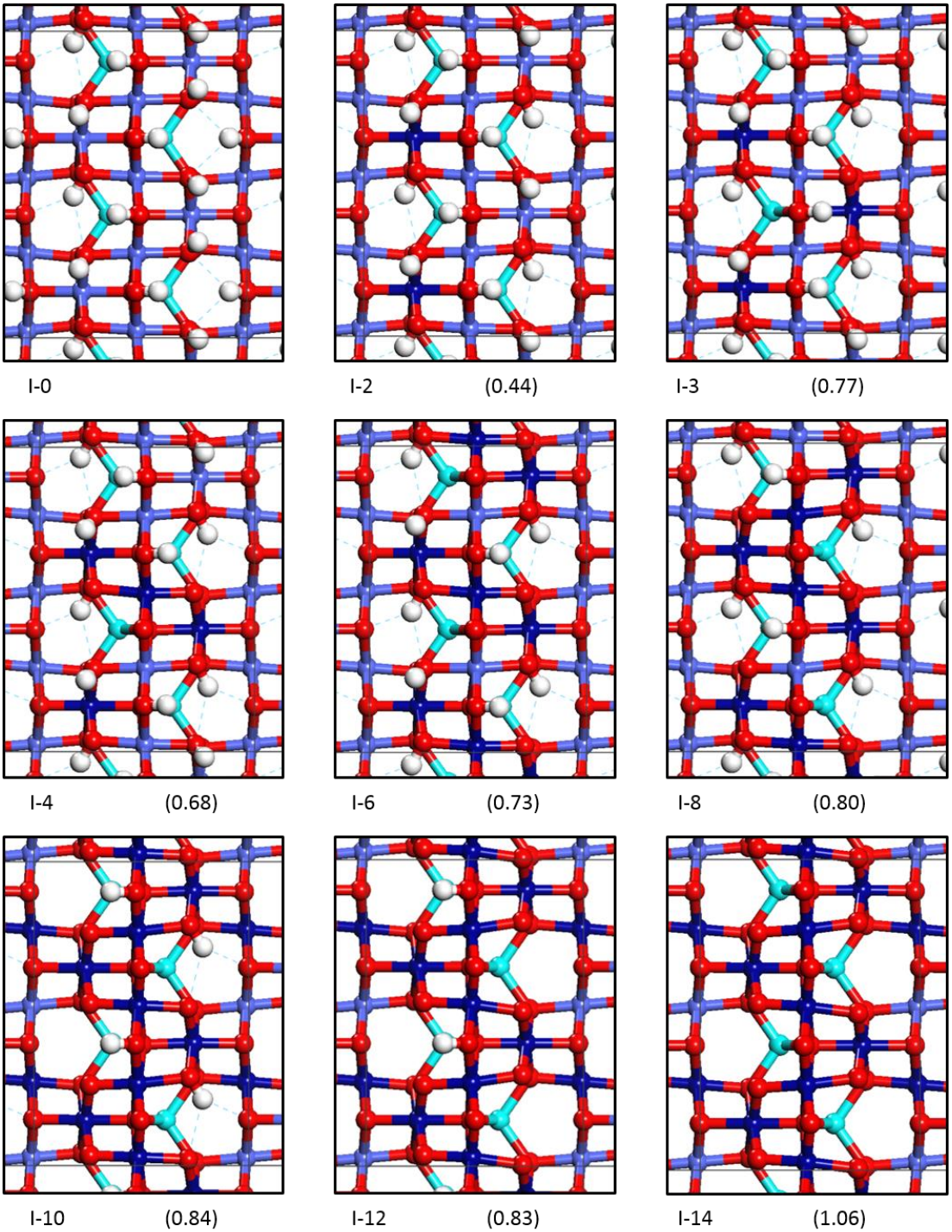

Figure S2. Structures of the states of the (110)-A dual-Co site. The numbers in parentheses are the oxidation potentials to form the surface from the preceding surface. Co cations are colored by oxidation state (light blue = Co(II), medium blue = Co(III), dark blue = Co(IV)).

Dominant intermediate and transition states of the (110)-A surface

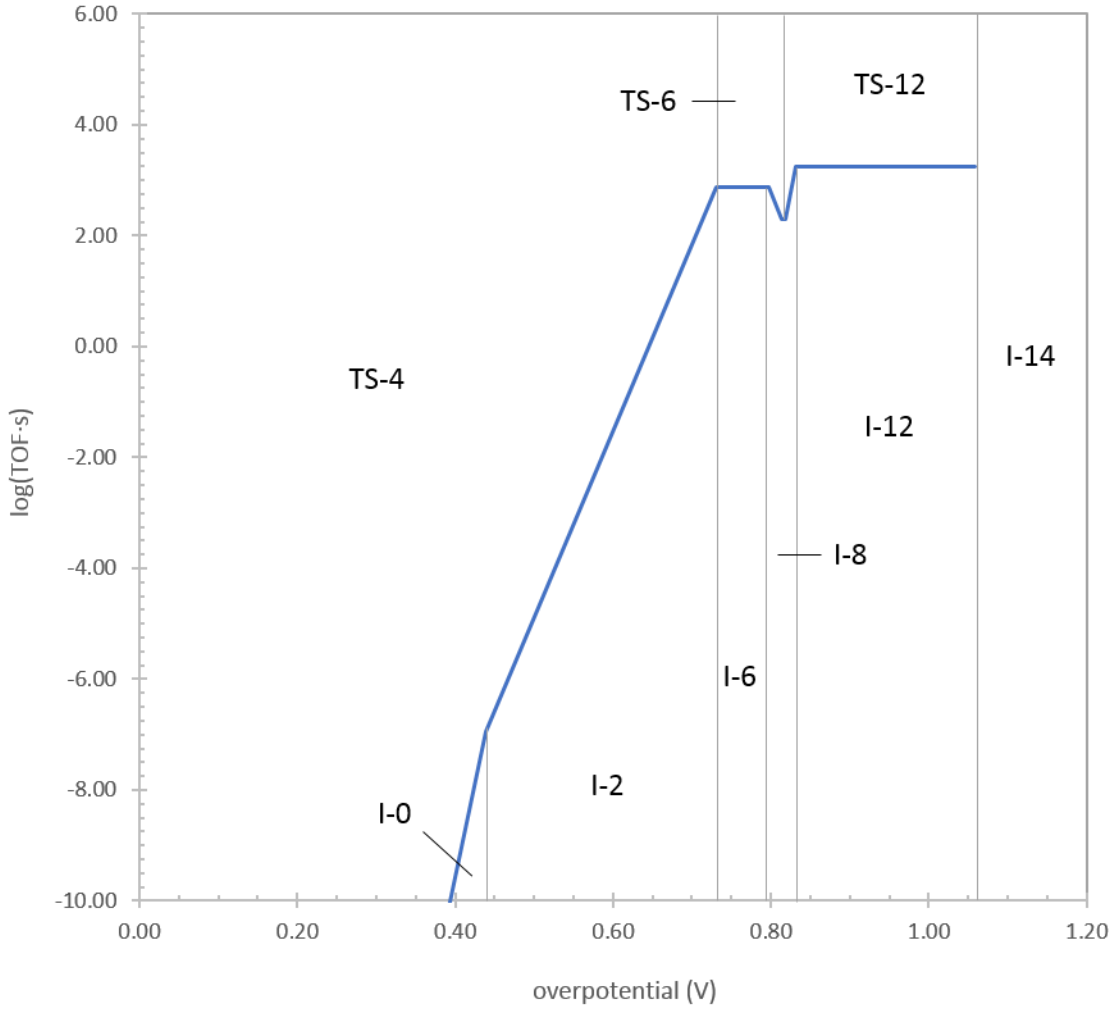

Figure S3. Dominant intermediate and transition states of the (110)-A surface as a function of overpotential. Structures of intermediate states are given in Figure S2.

Structures along the water addition pathway

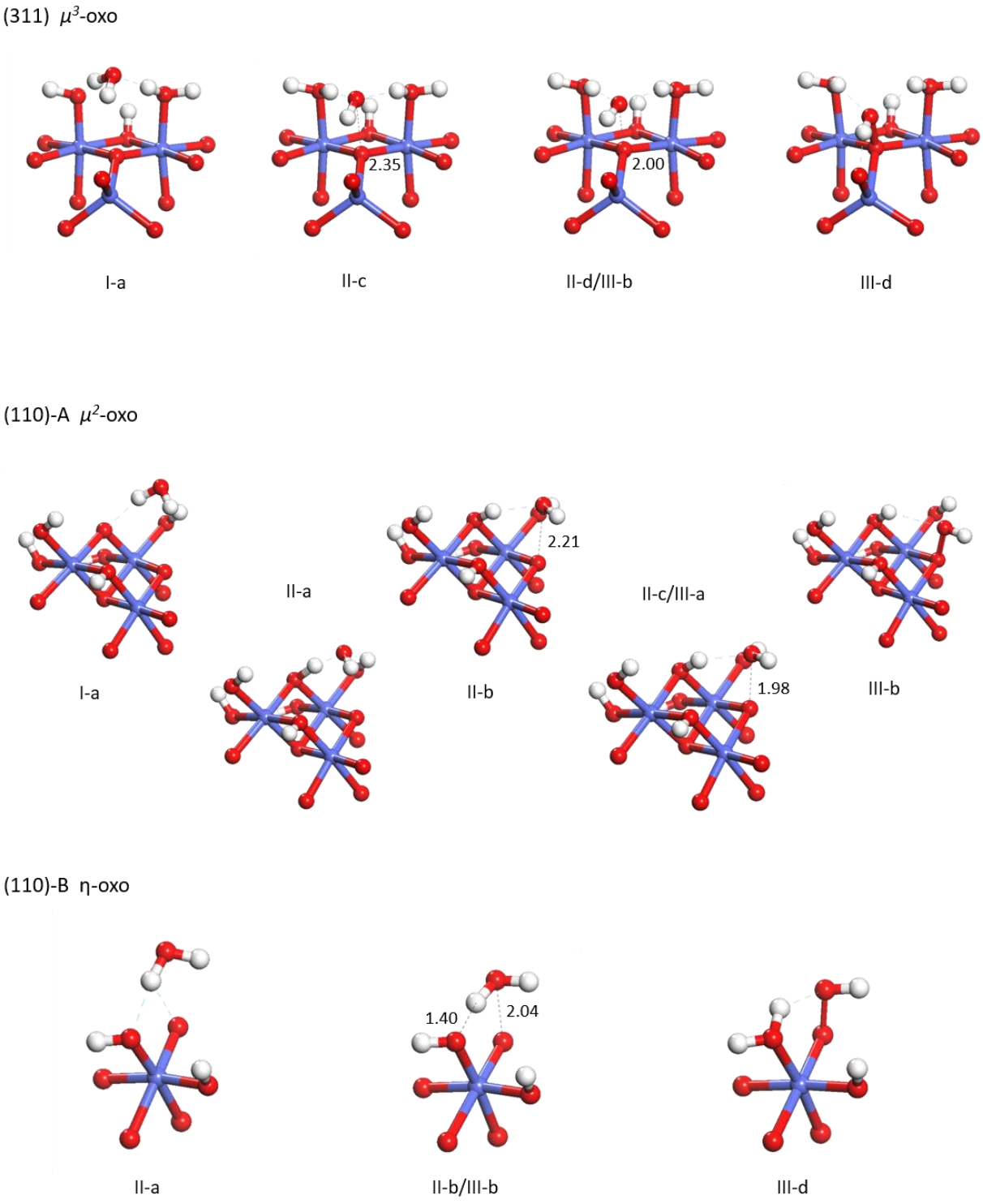

Figure S4. Structures along the water addition pathway corresponding to Figures 3 – 5 in the main text

Hole densities on structures along water addition pathway

(331)

I-a

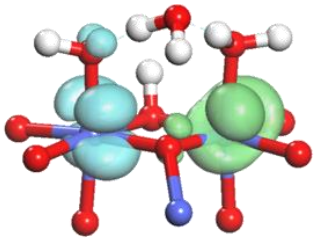

I-b

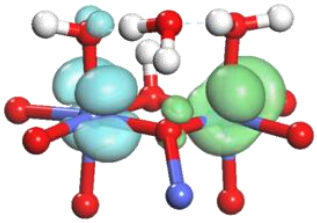

II-b

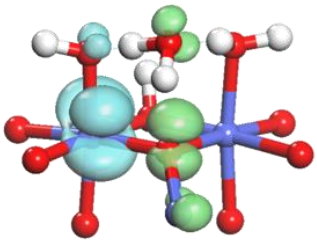

II-c

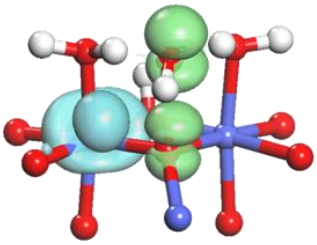

II-d

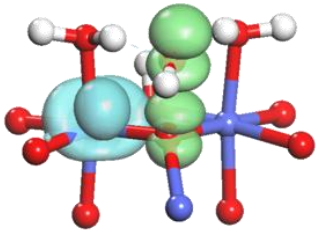

III-a

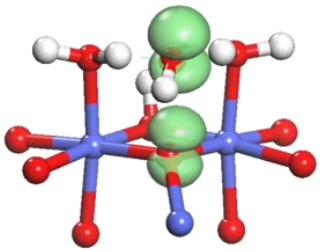

III-b

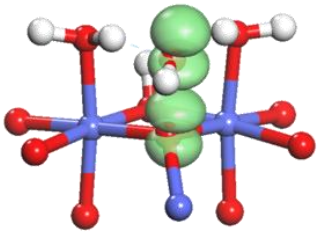

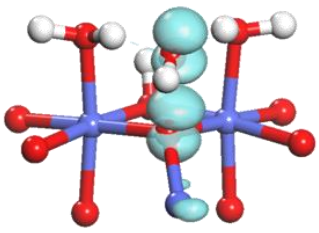

III-c

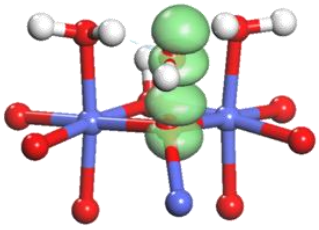

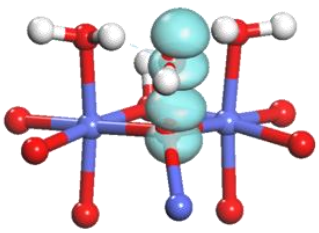

(110)-A

I-a

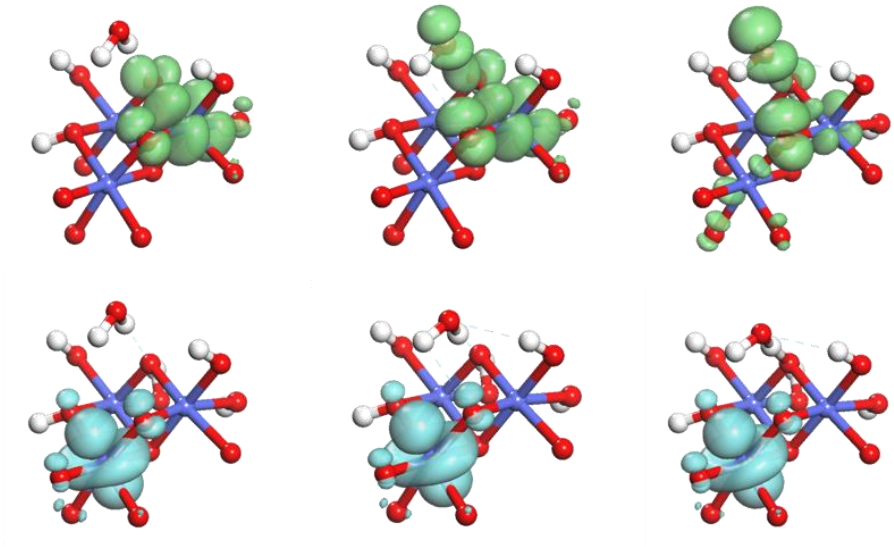

I-b

II-a

II-b

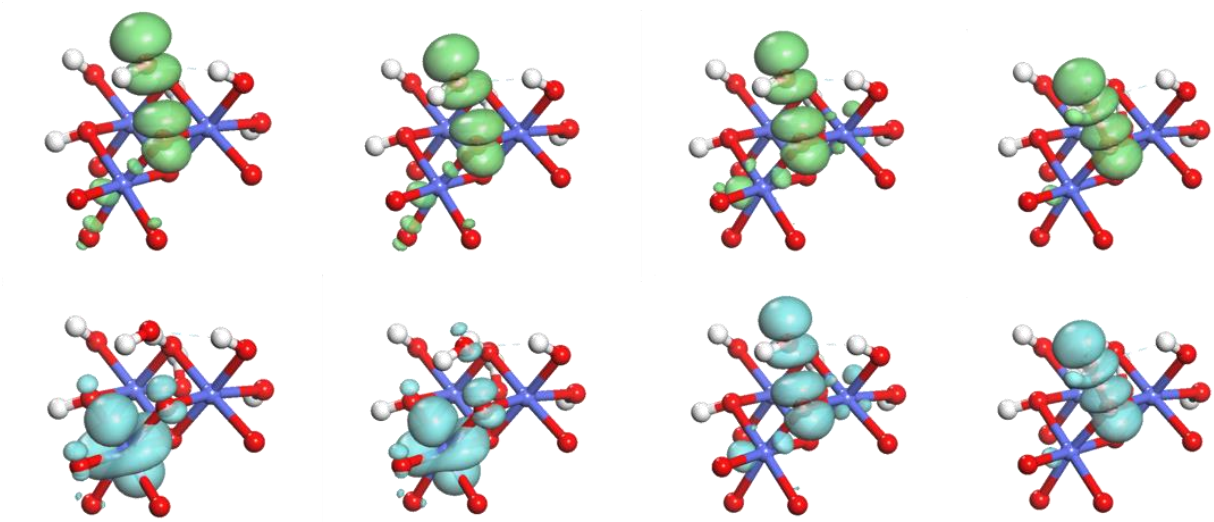

II-c

III-a

III-b

(110)-B

I

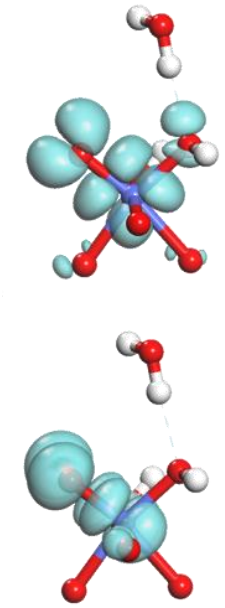

II-a

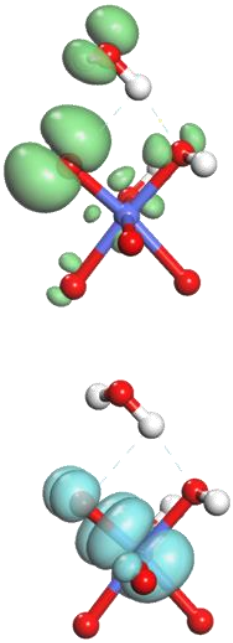

II-b

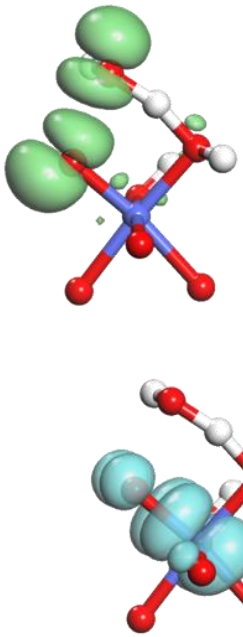

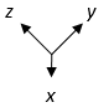

III-a

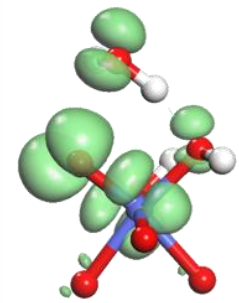

III-b

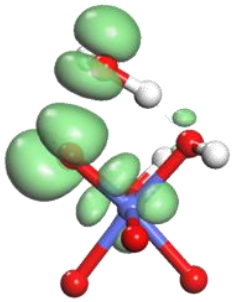

III-c

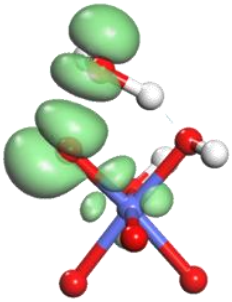

III-d

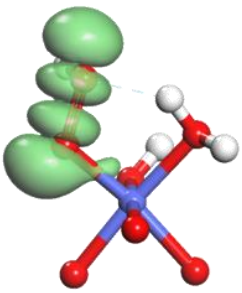

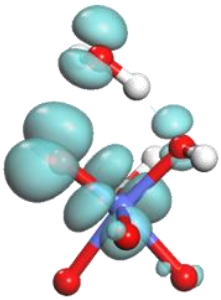

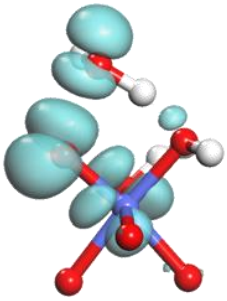

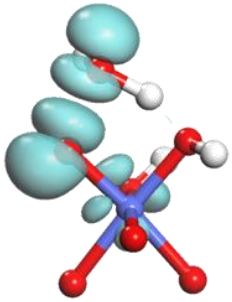

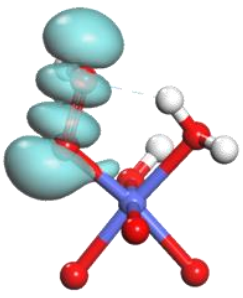

Figure S5. Hole densities for the structures along the water addition pathways in Figure 3 – 5 in the main text. (green = spin-up, blue = spin-down, grey = both spins)

Localized orbitals involving the oxo before and after O-O bond formation

(110)-B intermediate

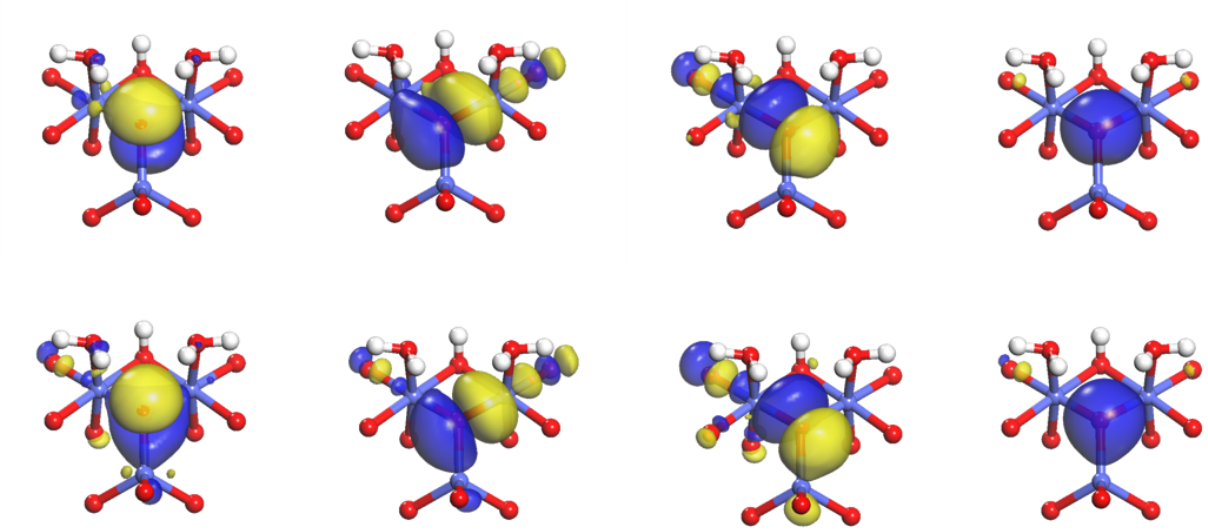

(110)-B product

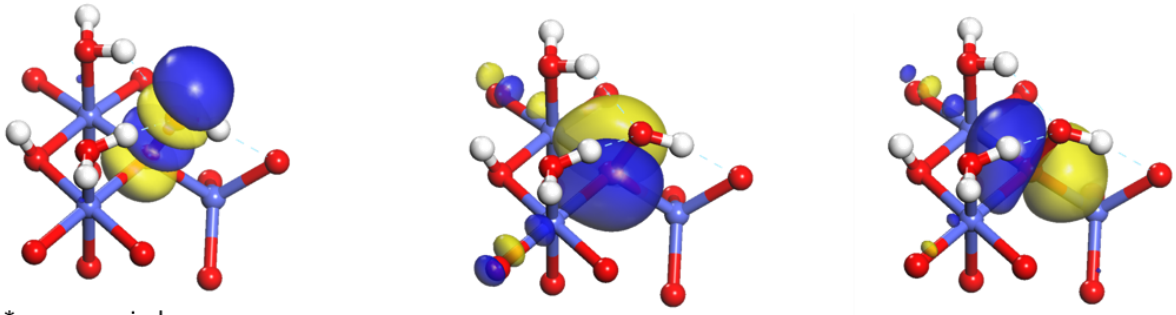

σ* - unoccupied

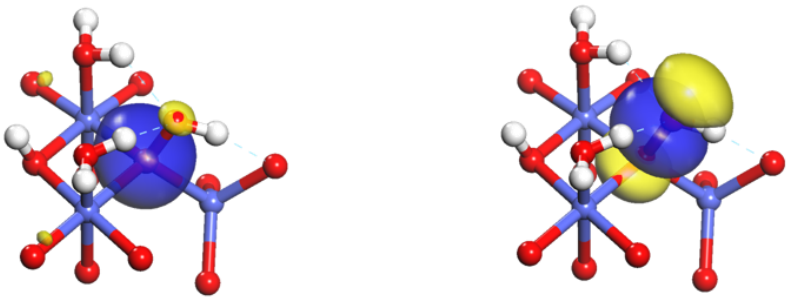

(110)-A intermediate

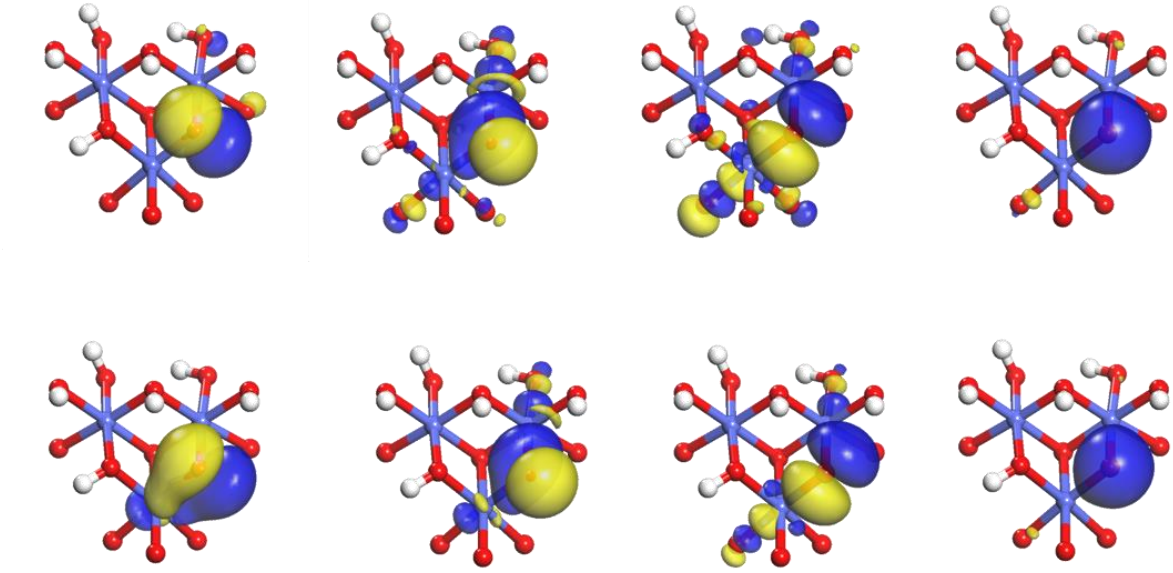

(110)-A product

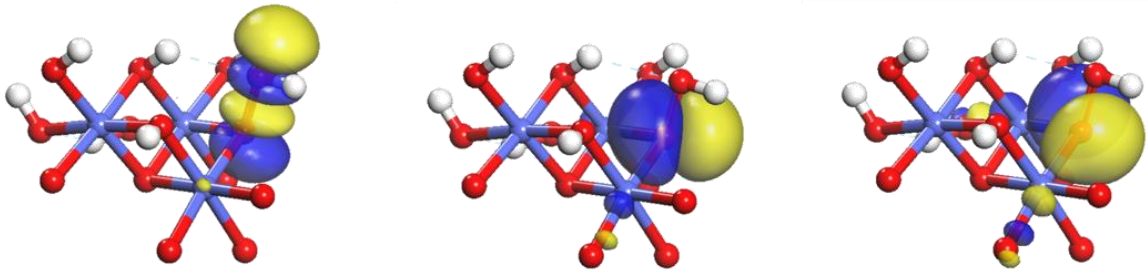

σ* - unoccupied

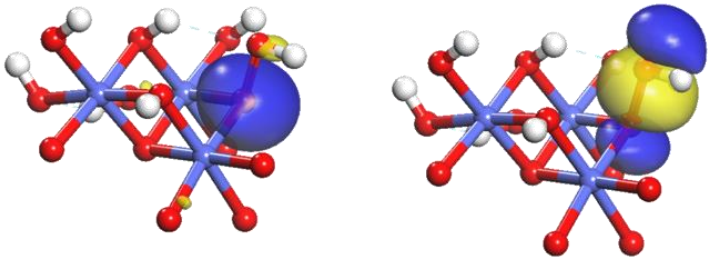

(110)-B intermediate

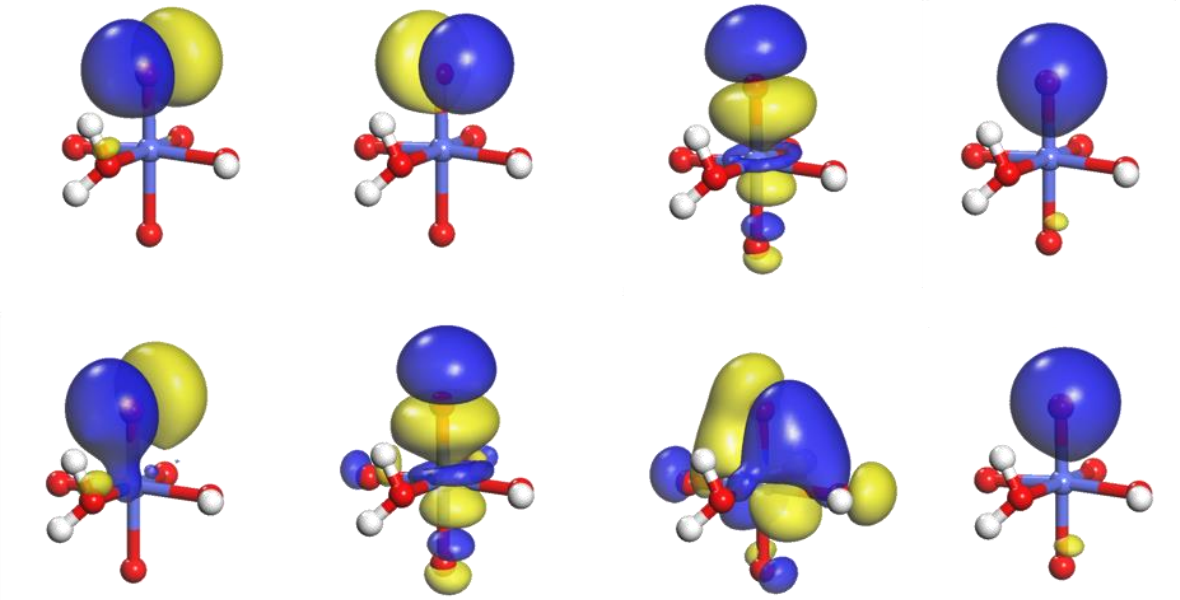

(110)-B product

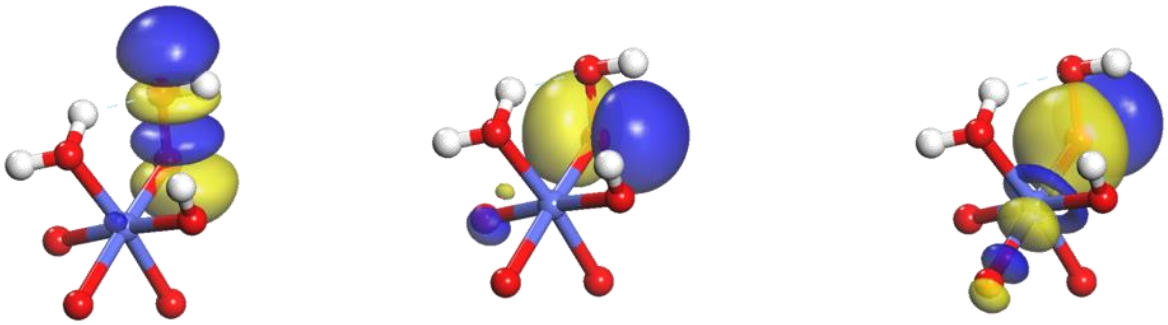

σ* - unoccupied

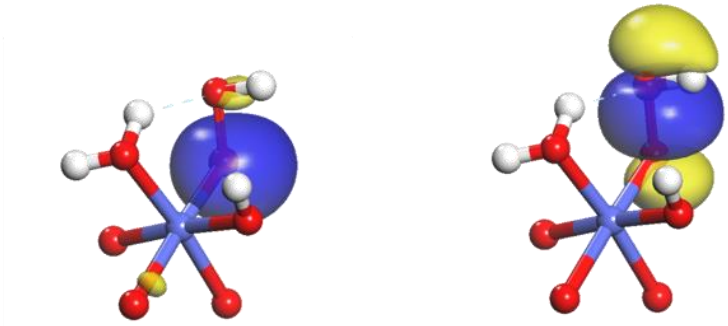

Figure S6. Orbitals localized on the oxo before and after O-O bond formation on the three sites. Four occupied orbitals of both spins are shown for the intermediate state preceding O-O formation. Four occupied orbitals and one unoccupied O-O antibonding orbital are shown for the product state after O-O formation; the spin-up and spin-down orbitals are nearly identical so only one set is shown.

Energies of constrained orbitals

Figure S7 below and Figure 8 in the main text display the energy of the constrained *2p* orbital on the oxo for different occupancies of this orbital. Since absolute energies in periodic calculations are not meaningful, it is necessary to choose an appropriate reference for these orbital energies. For this, we choose the unscreened energy of the constrained *3d* orbital on the Co cation. The unscreened energy ε_d^{us} is obtained from the self-consistent energy ε_d by correcting for differences in the electron population n_{Co} and spin moment m_{Co} on the Co cation from the reference values n_{Co}^0 and m_{Co}^0

(28)

$$\varepsilon_d^{us} = \varepsilon_d - \left(U_d - \frac{1}{2}J_d\right)\left(n_{Co} - n_{Co}^0\right) + \frac{1}{2}J_d m_{Co}$$

For the reference values, we used $n_{Co}^0 = 6.61$ and $m_{Co}^0 = 1.72$.

Eq. (28), as well as eq. (8) in the main text, require the effective Coulomb and exchange integrals for *2p* orbitals on the oxo (U_p and J_p) and *3d* orbitals on the Co (U_d and J_d). These integrals are obtained from the energies of the constrained orbitals (↑ = spin-up; ↓ = spin-down) for the calculation when the hole is on the Co ($q = 0$) and for the calculation when the hole is on the oxo ($q = 1$).

(29)

$$J_d = -\frac{\left[\varepsilon_d^{\uparrow}(q=1) - \varepsilon_d^{\downarrow}(q=1)\right] - \left[\varepsilon_d^{\uparrow}(q=0) - \varepsilon_d^{\downarrow}(q=0)\right]}{m_{Co}(q=1) - m_{Co}(q=0)}$$

(30)

$$2\,U_d - J_d = \frac{\left[\varepsilon_d^{\uparrow}(q=1) + \varepsilon_d^{\downarrow}(q=1)\right] - \left[\varepsilon_d^{\uparrow}(q=0) + \varepsilon_d^{\downarrow}(q=0)\right]}{n_{Co}(q=1) - n_{Co}(q=0)}$$

(31)

$$J_p = -\frac{\left[\varepsilon_p^{\uparrow}(q=1) - \varepsilon_p^{\downarrow}(q=1)\right] - \left[\varepsilon_p^{\uparrow}(q=0) - \varepsilon_p^{\downarrow}(q=0)\right]}{m_O(q=1) - m_O(q=0)}$$

(32)

$$2\,U_p - J_p = \frac{\left[\varepsilon_p^{\uparrow}(q=1) + \varepsilon_p^{\downarrow}(q=1)\right] - \left[\varepsilon_p^{\uparrow}(q=0) + \varepsilon_p^{\downarrow}(q=0)\right]}{n_O(q=1) - n_O(q=0)}$$

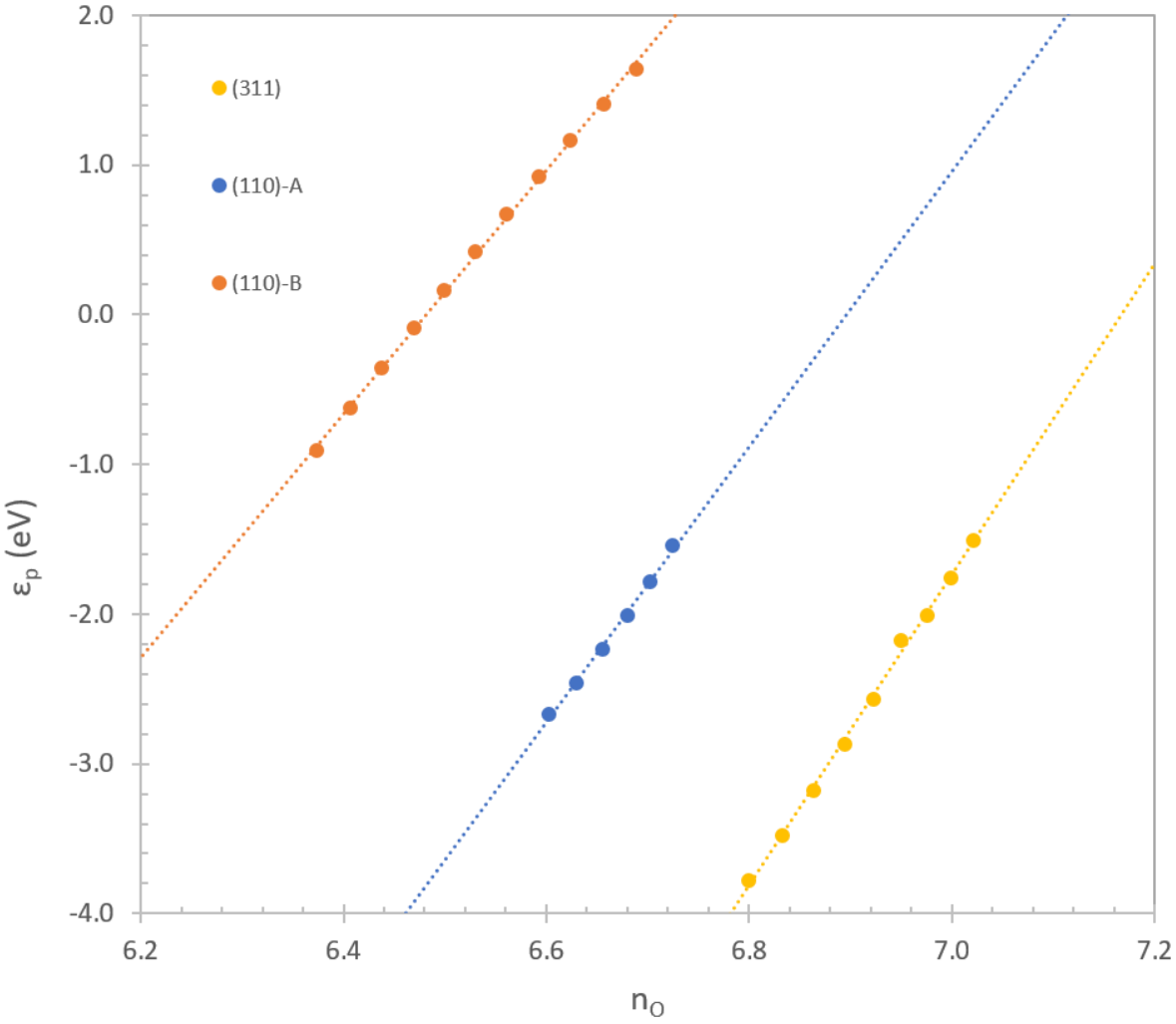

Figure S7. Energy of the constrained *2p* orbital on the oxo relative to the unscreened energy of the constrained *3d* orbital on the Co (given by eq. (28)) as a function of the electron population on the oxo

Correlations between energetic quantities associated with water addition

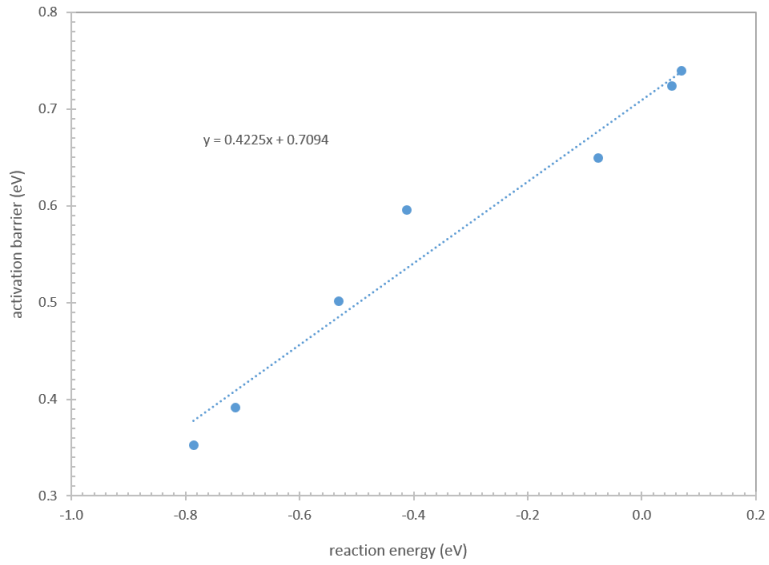

Figure S8. Brønsted-Evans-Polanyi correlation between the activation barrier of water addition and the reaction energy

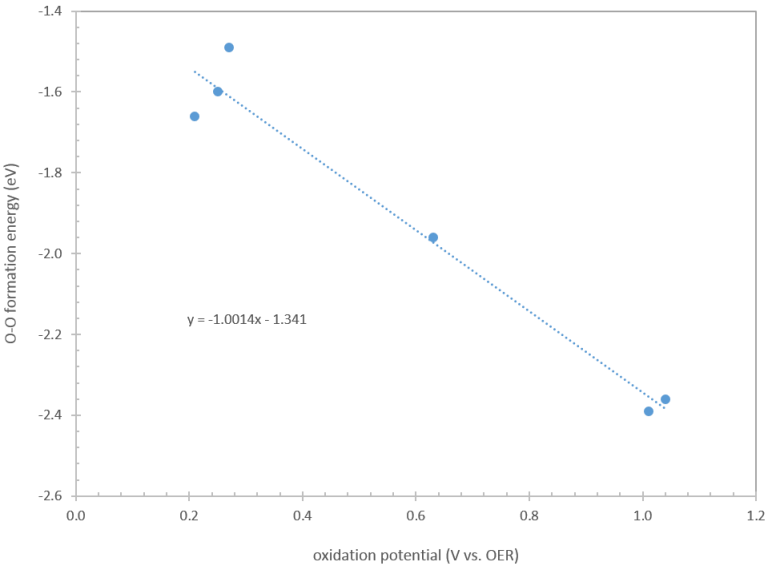

Figure S9. Correlation between O-O bond formation energy and the oxidation potential relating to the removal of a hydrogen atom from the hydroxo which forms the active oxo that undergoes water addition

Lower energy state on (001) surface

As discussed in the main text, a lower energy state with the same degree of oxidation as the active state exists on for the site on the (001) surface. In this state, shown in Figure S10, the proton on the μ^3-oxo in the active state is instead bound to the η-OH. Further details of this state are given in ref. 1.

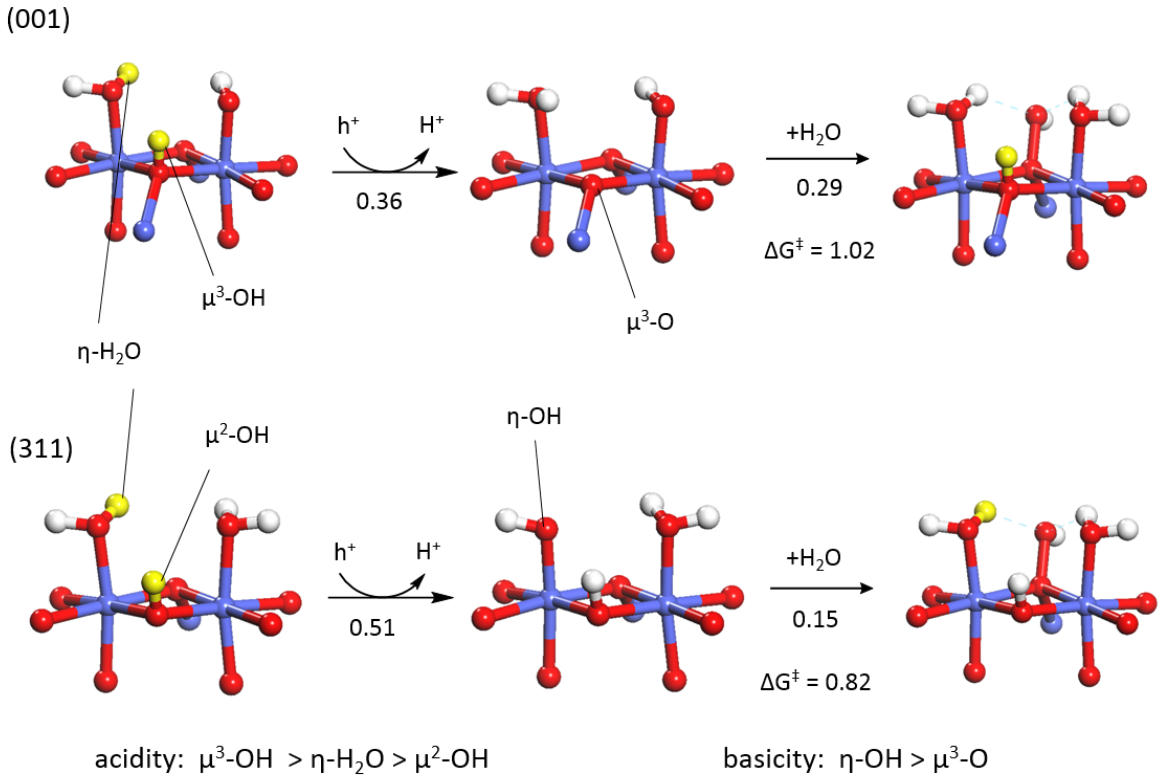

Figure S10. Comparison of the structures and energetics (eV at η = 0) of water addition to a dual-Co site on the (001) and (311) surfaces. The first step is the oxidation of the site by removal of an electron and proton and the second step is deprotonation of the attacking water and formation of the hydroperoxo. On the (001) site, the μ^3-OH deprotonates in the first step forming a μ^3-O that deprotonates the water in the next step. On the (311) site, this OH is coordinated by only two Co cations due to the location of the site on a step edge. This μ^2-OH is less acidic than the η-H_2O, which deprotonates instead to form an η-OH. The η-OH on the (311) site is more basic than the μ^3-O on the (001) site and more easily deprotonates the attacking water, leading to a less endothermic water addition with a lower barrier. (reproduced from ref. 1)

References

(1) Plaisance, C. P.; van Santen, R. A. *J. Am. Chem. Soc.* **2015**, *137* (46), 14660–14672.

(2) Kresse, G.; Furthmüller, J. *Phys. Rev. B* **1996**, *54* (16), 11169–11186.

(3) Kresse, G.; Furthmüller, J. *Comput. Mater. Sci.* **1996**, *6* (1), 15–50.

(4) Blöchl, P. E. *Phys. Rev. B* **1994**, *50* (24), 17953–17979.

(5) Kresse, G.; Joubert, D. *Phys. Rev. B* **1999**, *59* (3), 1758–1775.

(6) Hammer, B.; Hansen, L. B.; Nørskov, J. K. *Phys. Rev. B* **1999**, *59* (11), 7413–7421.

(7) Liechtenstein, A. I.; Anisimov, V. I.; Zaanen, J. *Phys. Rev. B* **1995**, *52* (8), R5467–R5470.

(8) Davidson, E. R. *J. Comput. Phys.* **1975**, *17* (1), 87–94.

(9) Pulay, P. *Chem. Phys. Lett.* **1980**, *73* (2), 393–398.

(10) Henkelman, G.; Jónsson, H. *J. Chem. Phys.* **1999**, *111* (15), 7010.

(11) Liu, X.; Prewitt, C. *Phys. Chem. Miner.* **1990**, *17* (2), 168–172.

(12) Nørskov, J. K.; Rossmeisl, J.; Logadottir, A.; Lindqvist, L.; Kitchin, J. R.; Bligaard, T.; Jónsson, H. *J. Phys. Chem. B* **2004**, *108* (46), 17886–17892.

(13) Rossmeisl, J.; Qu, Z.-W.; Zhu, H.; Kroes, G.-J.; Nørskov, J. K. *J. Electroanal. Chem.* **2007**, *607* (1-2), 83–89.

(14) Wang, L.; Maxisch, T.; Ceder, G. *Phys. Rev. B* **2006**, *73* (19), 195107.

(15) Henkelman, G.; Uberuaga, B. P.; Jónsson, H. *J. Chem. Phys.* **2000**, *113* (22), 9901.

(16) Henkelman, G.; Jónsson, H. *J. Chem. Phys.* **2000**, *113* (22), 9978.

(17) Halgren, T. A.; Lipscomb, W. N. *Chem. Phys. Lett.* **1977**, *49* (2), 225–232.

(18) Perdew, J. P.; Ruzsinszky, A.; Csonka, G. I.; Vydrov, O. A.; Scuseria, G. E.; Staroverov, V. N.; Tao, J. *Phys. Rev. A* **2007**, *76* (4), 040501.

(19) Qian, X.; Li, J.; Qi, L.; Wang, C.-Z.; Chan, T.-L.; Yao, Y.-X.; Ho, K.-M.; Yip, S. *Phys. Rev. B* **2008**, *78* (24), 245112.

(20) Löwdin, P.-O. *J. Chem. Phys.* **1950**, *18* (3), 365.